

Simulation analysis for the ultimate behavior of full-scale lead-rubber seismic isolation bearings



M. Kikuchi

Hokkaido University, Japan

I. D. Aiken

Seismic Isolation Engineering Inc., USA

A. Kasalanati

Dynamic Isolation Systems, USA

SUMMARY:

This paper presents a new three-dimensional analytical model for the accurate simulation of the ultimate behavior of full-scale lead-rubber seismic isolations bearings. The model comprises multiple shear springs at the mid-height and includes the interaction between biaxial shear and axial forces with nonlinear hysteresis. Severe loading tests for a range of different full-size lead-rubber bearings were conducted to obtain data to validate the analytical model. The test programs included a variety of different loading patterns, such as monotonic, cyclic, and horizontal bidirectional earthquake ground motions. Buckling or stiffening behavior was observed under large shear deformations and high axial loads. Very good agreement between the experimental and analytical results was obtained, indicating that the model is useful for the prediction of the seismic response of isolated structures under severe earthquake ground motions.

Keywords: Seismic isolation, elastomeric isolation bearing, nonlinear analysis

1. INTRODUCTION

Seismic isolation is the most effective technology for protecting structures from the damaging effects of earthquakes. The concept of seismic isolation is to move the fundamental period of a structure away from the predominant period of the ground motion through the introduction of flexible supports at the foundation level. It has been extensively used worldwide over the last three decades. Numerous earthquakes have confirmed the good response of seismically-isolated buildings, including the fully operational performance of isolated hospitals in the 1994 Northridge Earthquake, USA, and the 2011 Great Tohoku Earthquake, Japan, amongst others. Seismic isolation has been proven to provide the highest level of seismic protection possible for buildings and other structures.

The widespread use of seismic isolation has necessitated a better understanding of the ultimate behavior of isolation devices under large shear deformations or high compressive stresses. Elastomeric isolation bearings exhibit strongly nonlinear behavior, such as stiffening or buckling influenced by axial loading under large deformations. For the accurate prediction of the ultimate behavior of isolation devices, the authors have developed a series of mechanical models. The initial prototype model was developed in two dimensions, which comprised shear and axial springs at the mid-height and a series of axial springs at the top and bottom boundaries of the model. The latest model was developed by expanding the prototype model to three dimensions (Kikuchi *et al.*, 2010). It comprises multiple shear springs at the mid-height and includes interaction between biaxial shear and axial forces with non-linear hysteresis. In the early stage of development of the model it was validated by showing that it could accurately predict the behavior of reduced-scale isolation bearings, with diameters of about 20 cm. The validation of numerical models with extreme loading data from testing of full-size isolation bearings, however, has generally not often been done, because of the capacity limitations of most test facilities and the limited opportunities to perform such tests. The authors have conducted severe loading tests of full-size lead-rubber bearings, and the data obtained from these tests presented an unusual opportunity for further validation of the analytical model. The diameter of the full-size

bearings tested was approximately 1.0 meters. The test programs included a variety of different loading patterns, such as cyclic and horizontal bidirectional earthquake ground motions. Buckling or stiffening behaviors were observed in the tests under large shear deformations and high axial loads. The newly developed model initially assumed a uniform distribution of the compression modulus over the entire cross section of a bearing. While the assumption of uniform distribution was valid for the reduced-scale isolation bearings; however, it failed to accurately predict the behavior for the full-scale bearings. Therefore, in this paper, a refinement is introduced for the calculation of the compression modulus to include the influence of the bulk modulus compressibility and the shape of the bearing cross section.

2. MECHANICAL MODEL

Fig. 2.1 shows the mechanical model proposed to simulate the behavior of elastomeric isolation bearings. The model comprises multiple shear springs (MSSs) and an axial spring at the mid-height and two series of axial springs at the top and bottom boundaries. The MSS model is used in the mechanical model to represent the biaxial behavior of the elastomeric isolation bearings, which consists of a series of identical shear springs arranged radially to represent isotropic behavior in the horizontal plane (Wada and Hirose, 1989). Each spring in the series of axial springs at the top and bottom boundaries is a uniaxial, nonlinear spring and represents an individual fiber of the bearing's cross-sectional area. When this collection of springs is combined in the model, the nonlinear interaction behavior is achieved. The rigid columns, which represent the height of the bearing, are combined between the top and bottom series of axial springs and mid-height MSSs and the axial spring.

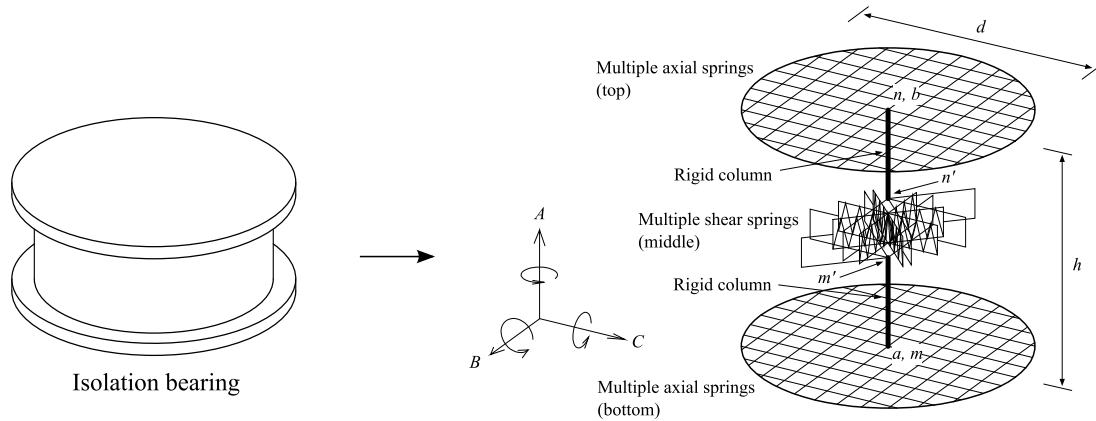


Figure 2.1. Three-dimensional multiple-spring mechanical model

The definition of the forces and displacements on the model is shown in Fig. 2.2. There are six displacement degrees of freedom – three translations and three rotations – at the external nodes, a and b . The internal nodes, m and n , have three displacement degrees of freedom: translation A and rotations B and C . The displacements for translations B and C and rotation A of the internal node, m , are equal to those of the external node, a . The same definition for nodes a and m is made for nodes b and n . By using incremental displacements of nodes a and m and assuming that plane sections remain plane, the relationship between the incremental force vector, $\Delta \mathbf{f}_{am}$, and the incremental displacement vector, $\Delta \mathbf{u}_{am}$, on nodes a and m can be obtained as follows:

$$\Delta \mathbf{f}_{am} = \mathbf{K}_{am} \cdot \Delta \mathbf{u}_{am} \quad (2.1)$$

where

$$\Delta \mathbf{u}_{am} = \left\{ \Delta \delta_{Aa} \quad \Delta \theta_{Ba} \quad \Delta \theta_{Ca} \quad \Delta \delta_{Am} \quad \Delta \theta_{Bm} \quad \Delta \theta_{Cm} \right\}^T$$

$$\Delta \mathbf{f}_{am} = \left\{ \Delta f_{Aa} \quad \Delta m_{Ba} \quad \Delta m_{Ca} \quad \Delta f_{Am} \quad \Delta m_{Bm} \quad \Delta m_{Cm} \right\}^T$$

where \mathbf{K}_{bn} is the stiffness matrix, $\Delta \mathbf{f}_{bn}$ is the incremental force vector, and $\Delta \mathbf{u}_{bn}$ is the incremental displacement vector of nodes b and n .

Now consider the force-displacement relationships for the multiple shear springs and the axial spring at the mid-height of the model. The force-displacement relationship on nodes n' and m' in Fig. 2.2, which excludes the rigid columns, may be expressed as follows:

$$\Delta \mathbf{f}'_{mn} = \mathbf{K}'_{mn} \cdot \Delta \mathbf{u}'_{mn} \quad (2.3)$$

where

$$\Delta \mathbf{f}'_{mn} = \left\{ \Delta f'_{Am} \quad \Delta f'_{Bm} \quad \Delta f'_{Cm} \quad \Delta f'_{An} \quad \Delta f'_{Bn} \quad \Delta f'_{Cn} \right\}^T$$

$$\Delta \mathbf{u}'_{mn} = \left\{ \Delta \delta'_{Am} \quad \Delta \delta'_{Bm} \quad \Delta \delta'_{Cm} \quad \Delta \delta'_{An} \quad \Delta \delta'_{Bn} \quad \Delta \delta'_{Cn} \right\}^T$$

$$\mathbf{K}'_{mn} = \begin{bmatrix} k_N & 0 & 0 & -k_N & 0 & 0 \\ & {}_1k'_{mn} & {}_2k'_{mn} & 0 & -{}_1k'_{mn} & -{}_2k'_{mn} \\ & & {}_3k'_{mn} & 0 & -{}_2k'_{mn} & -{}_3k'_{mn} \\ & & & k_N & 0 & 0 \\ & \text{symm.} & & & {}_1k'_{mn} & {}_2k'_{mn} \\ & & & & & {}_3k'_{mn} \end{bmatrix}, \quad \begin{aligned} {}_1k'_{mn} &= \sum_j k_S \cos^2_j \varphi, \\ {}_2k'_{mn} &= \sum_j k_S \cos_j \varphi \sin_j \varphi, \\ {}_3k'_{mn} &= \sum_j k_S \sin^2_j \varphi \end{aligned}$$

where ${}_j k_S$ is the tangential stiffness, ${}_j \varphi$ is the angle to the B axis of the j -th shear spring (Fig. 2.4), and k_N is the stiffness of the axial spring at the mid-height.

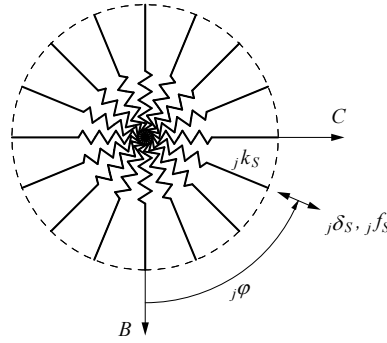


Figure 2.4. Multiple shear springs at the mid-height

In order to convert the force-displacement relationship of nodes m' and n' , expressed by Eqn. (2.3), to nodes m and n , which includes the rigid columns, a transformation matrix is used. Taking the geometrical relationships of the deformations, the force equilibrium condition, and the P - Δ effect into account gives the transformation matrix. Fig. 2.5 shows the geometrical relationships of the deformations and the forces in the A - C plane. Let ${}_{AC} \mathbf{T}$ be the transformation matrix in the A - C plane, $\Delta_{AC} \mathbf{u}'_{mn}$ and $\Delta_{AC} \mathbf{f}'_{mn}$ be the displacements and forces on nodes m' and n' , and $\Delta_{AC} \mathbf{u}_{mn}$ and $\Delta_{AC} \mathbf{f}_{mn}$ be those on nodes m and n , respectively. The transformation of the displacements and forces may be expressed by

$$\Delta_{AC} \mathbf{u}'_{mn} = {}_{AC} \mathbf{T} \cdot \Delta_{AC} \mathbf{u}_{mn} \quad (2.4)$$

$$\Delta_{AC} \mathbf{f}_{mn} = {}_{AC} \mathbf{T}^T \cdot \Delta_{AC} \mathbf{f}'_{mn} \quad (2.5)$$

where

$$\Delta_{AC} \mathbf{u}'_{mn} = \left\{ \Delta \delta'_{Am} \quad \Delta \delta'_{Ca} \quad \Delta \theta'_{Bm} \quad \Delta \delta'_{An} \quad \Delta \delta'_{Cb} \quad \Delta \theta'_{Bn} \right\}^T$$

$$\begin{aligned}\Delta \mathbf{f}_{ex} &= \{\Delta f_{Aa} \quad \Delta f_{Ba} \quad \Delta f_{Ca} \quad \Delta m_{Aa} \quad \Delta m_{Ba} \quad \Delta m_{Ca} \quad \Delta f_{Ab} \quad \Delta f_{Bb} \quad \Delta f_{Cb} \quad \Delta m_{Ab} \quad \Delta m_{Bb} \quad \Delta m_{Cb}\}^T \\ \Delta \mathbf{f}_{in} &= \{\Delta f_{Am} \quad \Delta m_{Bm} \quad \Delta m_{Cm} \quad \Delta f_{An} \quad \Delta m_{Bn} \quad \Delta m_{Cn}\}^T \\ \Delta \mathbf{u}_{ex} &= \{\Delta \delta_{Aa} \quad \Delta \delta_{Ba} \quad \Delta \delta_{Ca} \quad \Delta \theta_{Aa} \quad \Delta \theta_{Ba} \quad \Delta \theta_{Ca} \quad \Delta \delta_{Ab} \quad \Delta \delta_{Bb} \quad \Delta \delta_{Cb} \quad \Delta \theta_{Ab} \quad \Delta \theta_{Bb} \quad \Delta \theta_{Cb}\}^T \\ \Delta \mathbf{u}_{in} &= \{\Delta \delta_{Am} \quad \Delta \theta_{Bm} \quad \Delta \theta_{Cm} \quad \Delta \delta_{An} \quad \Delta \theta_{Bn} \quad \Delta \theta_{Cn}\}^T\end{aligned}$$

and $\Delta \mathbf{f}_{ex}$ and $\Delta \mathbf{u}_{ex}$ are the incremental forces and displacements on the external nodes, a and b , and $\Delta \mathbf{f}_{in}$ and $\Delta \mathbf{u}_{in}$ are those on the internal nodes, m and n , respectively.

3. HYSTERESIS MODEL

The shear hysteresis model previously developed by the authors, which is capable of predicting the behavior of elastomeric isolation bearings under large shear deformations, is applied to each spring in the MSS model (Kikuchi and Aiken, 1997). In the proposed mechanical model, the reduction of horizontal stiffness and eventual buckling behavior due to high axial loading is represented by the interaction between the shear and axial forces in the tilted MSS model and the axial springs. Therefore, the hysteresis properties to be used for the shear springs in the MSS model should be those under low compressive stress (ideally under zero compressive stress). The shear force-shear strain relationship up to 400% strain used for the MSS model is shown in Fig. 3.1(a) (Kikuchi *et al.*, 2010).

The stress-strain relationship for the series of axial springs at the top and bottom boundaries is shown in Fig. 3.1(b). In general, a laminated rubber bearing exhibits high stiffness and yielding stress in the compression region and low stiffness and yielding stress in the tension region. The relationship between vertical strain and stress is antisymmetric. The behavior represented by the model shown in Fig. 3.1(b) is generally accepted for the nonlinear vertical behavior of elastomeric isolation bearings.

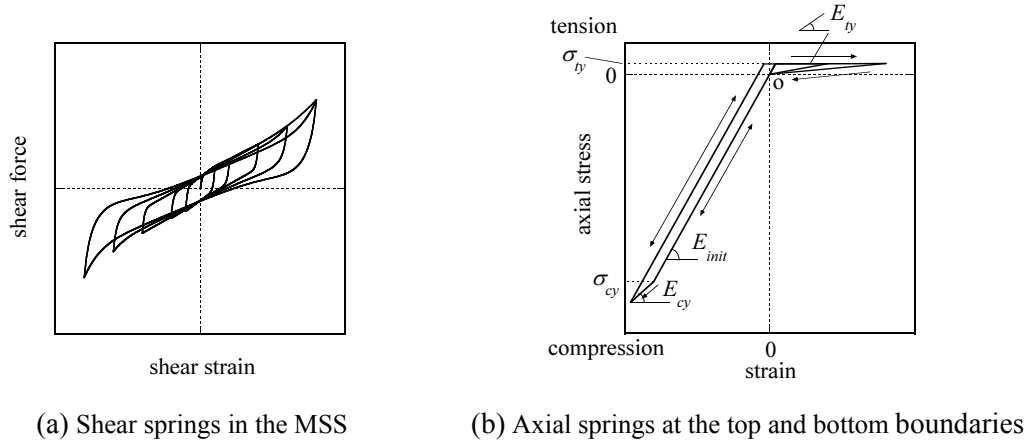


Figure 3.1. Hysteresis models

The previously developed model assumed a uniform distribution of the initial compression modulus, E_{init} , over the cross section of a circular bearing, as shown in Fig. 3.2(a), which is given by Eqn. (3.1),

$$E_{init} = \frac{E_0(1 + 2\kappa S_1^2)K}{E_0(1 + 2\kappa S_1^2) + K} \quad (3.1)$$

where E_0 is the Young's modulus of rubber, κ is a constant related to the rubber's hardness, S_1 is the rubber's shape factor, and K is the bulk modulus of rubber.

In the new model presented herein, an improvement is made in the calculation of the initial compression modulus. The distribution of the compression modulus is considered as shown in Fig.

3.2(b). The compression modulus is computed from Eqn. (3.2), which is expressed as a function of the distance, r , from the centroid of the bearing cross section. Eqn. (3.2) is the exact solution of the governing equation of the pressure distribution considering the influence of the bulk compressibility (Kelly, 1997),

$$E_{init}(r) = K \left\{ 1 - \frac{I_0(\lambda r)}{I_0(\lambda R)} \right\} \quad (3.2)$$

where

$$\lambda = \sqrt{\frac{12G}{Kt^2}}$$

and I_0 is the modified Bessel function of the first kind of order zero, G is the shear modulus of rubber, and t is the thickness of the rubber pad.

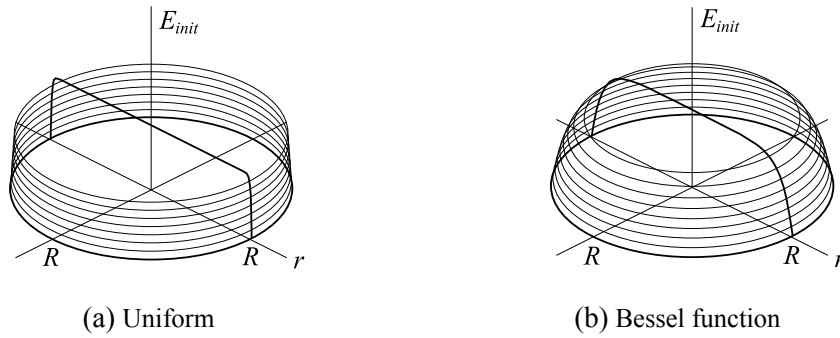


Figure 3.2. Distribution of initial compression modulus

The hysteresis model shown in Fig. 3.1(b) defines the tangent compression modulus. The stiffness of each axial spring, ${}_i k_{Na}$, at the top and bottom boundaries is obtained from

$${}_i k_{Na} = \frac{{}_i E \cdot {}_i A}{l} \quad (3.3)$$

where ${}_i E$ is the tangent compression modulus of the i -th spring, ${}_i A$ is the incremental area corresponding to the i -th spring, and l is the imaginary length of the spring. One half of the total height of the rubber in the bearing is usually used for this imaginary length.

4. SIMULATION ANALYSES

Tests of large lead-rubber bearings were conducted to investigate their mechanical characteristics under severe loading conditions (Sherstobitoff *et al.*, 2008). Fig. 4.1 shows the dimensions of the lead-rubber bearings used for the tests. The tests were conducted at the University of San Diego SRMD Testing Facility, which is the most sophisticated facility of its type in the world for testing seismic isolation devices. The test program included a variety of different loading patterns, such as monotonic, cyclic, and horizontal bidirectional earthquake ground motions. The results of two different types of tests were selected to compare against the results given by the analytical model (Table 4.1).

The parameters used for the simulation analyses are summarized in Table 4.2. Some of these parameters were determined by initially evaluated test results for other types of elastomeric isolation bearings. From previous analyses it was understood that the convergence of the model depends on the cross-section discretization selected for the analysis. A 50x50 grid of axial springs was selected as appropriate for the bearing design. Three different analysis cases for each test were performed in order to demonstrate the validity of the refinement introduced to the mechanical model (Table 4.3). The

loading sequence used for the analyses was exactly the same as for the tests. Initially, the axial load was applied to the top of the model, then the test shear displacement history was applied.

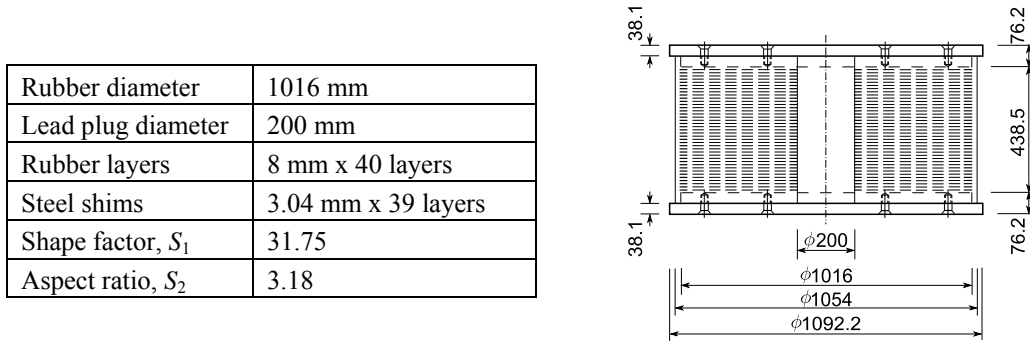


Figure 4.1. Lead-rubber bearing design details

Table 4.1. Tests selected for analytical comparison

Test 1	Shear capacity limit-state test Unidirectional, one cycle Constant axial load (stress): 14,000 kN (17.3 MPa) Peak displacement (shear strain): 320 mm (100%), 640 mm (200%) Peak velocity: 63.5 mm/s
Test 2	Bidirectional, dynamic earthquake input test Constant axial load (stress): 14,000 kN (17.3 MPa) 1999 Kocaeli Earthquake X & Y displacement time histories, real time

Table 4.2. Bearing parameters used for the simulation analyses

Increments in the top and bottom boundaries	50 x 50
Number of springs in MSS model	8
Shear modulus of rubber, G	0.49 MPa
Young's modulus of rubber, E_0	1.47 MPa
Bulk modulus of rubber, K	1960 MPa
Constant related to rubber hardness, κ	0.85
Tension yield stress, σ_{ty}	1 MPa
Tension yield modulus, E_{ty}	$E_{init}/100$
Compression yield stress, σ_{cy}	100 MPa
Compression post-yield modulus, E_{cy}	$E_{init}/2$

Table 4.3. Analysis cases

Case 1	P- Δ effect not considered
Case 2	P- Δ effect considered, uniform distribution of compression modulus
Case 3	P- Δ effect considered, Bessel function distribution of compression modulus

The experimental results shown in Fig. 4.2 were obtained from the shear capacity limit-state tests as summarized in Table 4.2. The axial load applied to the isolator in this test was approximately 26% greater than the critical load for the 640 mm shear displacement (11,095 kN). Consequently, the isolator hysteresis exhibits negative incremental stiffness at shear strains beyond about 100%. The analytical results are also shown in Fig. 4.2. The experimental hysteresis loop at 100% peak shear strain doesn't exhibit negative incremental stiffness, therefore all three analysis cases show good agreement with the test result. However, the analytical hysteresis loops don't agree well with the test results at 200% peak shear strain if the P- Δ effect is not considered, as shown in Fig. 4.2(a). The hysteresis loops obtained from both of Cases 2 and 3 exhibit negative incremental stiffness. Case 3

predicts the behavior more accurately than Case 2, and shows good agreement with the test result. This shows that the refinements to the analytical model have improved the capability to accurately predict bearing behavior under extreme loading conditions. The distribution of the compression modulus over the cross-section leads directly to the geometric moment of inertia. The accurate representation of compressive behavior is important, because the bending stiffness has a strong influence on the inclination of the shear springs at the mid-height of the model. The Bessel function distribution of the compression modulus as shown in Fig. 3.2(b) produces lower bending stiffness than does the uniform distribution of the compression modulus. Consequently the refined compression modulus distribution improves the accuracy of the simulation analyses.

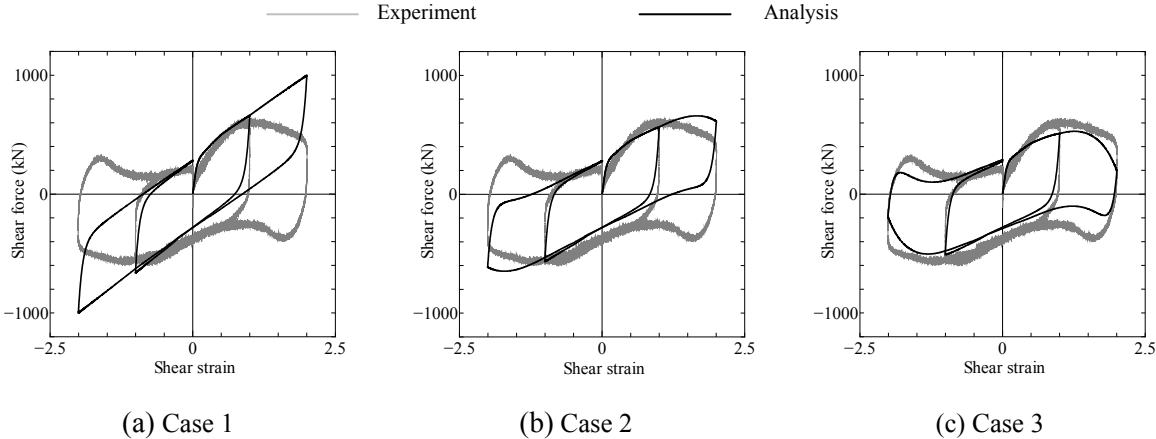


Figure 4.2. Comparison of analytical and test results for uni-directional cyclic loading with high compressive stress (17.3 MPa), Test 1

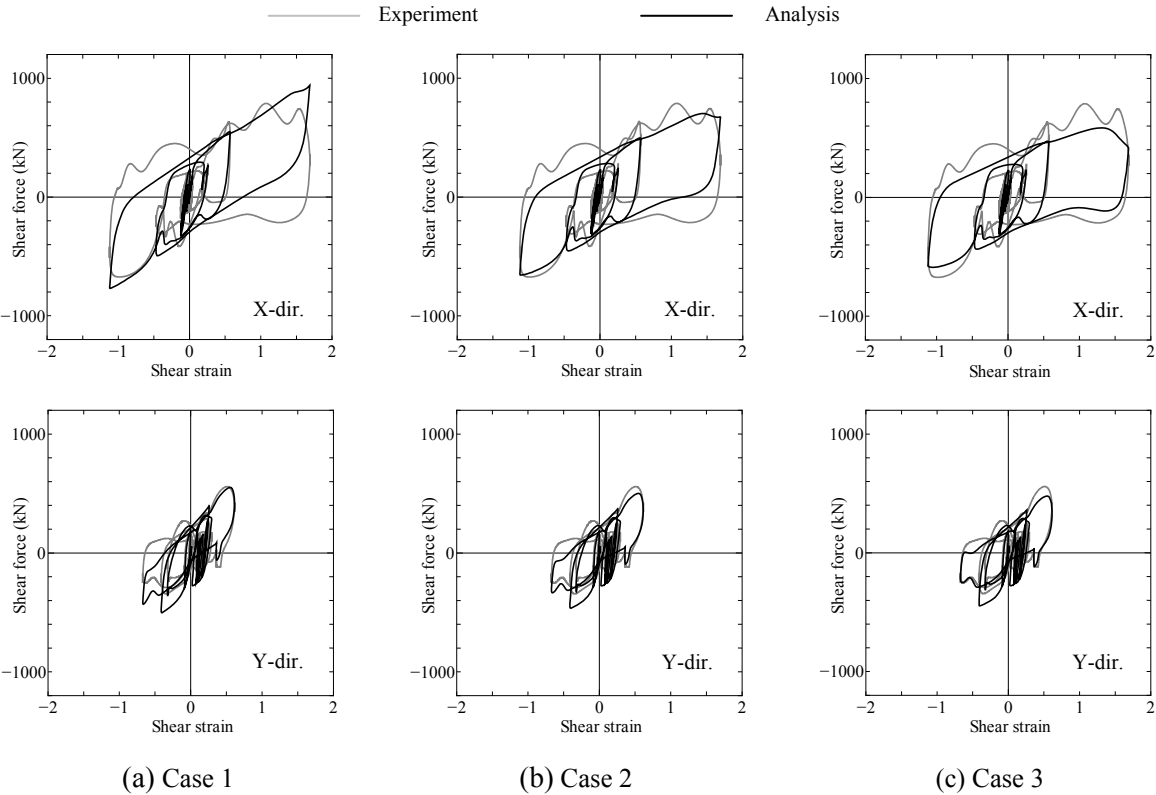


Figure 4.3. Comparison of analytical and test results for bi-directional dynamic earthquake input, with high compressive stress (17.3 MPa), Test 2

The experimental results shown in Fig. 4.3 were obtained from the bi-directional, dynamic earthquake tests described in Table 4.2. An axial load of 14,000 kN was applied, then the bearing was subjected to bi-directional horizontal displacement time histories determined from the seismic response analyses of an isolated tower structure subjected to ground motions from the 1999 Kocaeli, Turkey, M_w 7.4 Earthquake (Sherstobitoff *et al.*, 2008). The peak test displacement and velocity were 528 mm and 785 mm/s, respectively, and the total duration of loading was 22 s. Such as loading can be categorized as a severe, high-speed loading test. Slight negative incremental stiffness is observed in the X-direction hysteresis. The analytical results are also shown in Fig. 4.3, and it can be seen that Case 3 accurately predicts the test bi-directional hysteresis behaviour.

5. CONCLUSIONS

A three-dimensional mechanical model for seismic isolation bearings under large shear deformations and high axial loads has been developed. The model comprises MSSs at its mid-height and a series of axial springs at the top and bottom boundaries. The model can capture the interaction between multi-directional shear displacement and axial force, non-linear hysteresis, and the dependence on vertical load by considering both material and geometrical nonlinearities in its formulation. The present work has introduced a refinement for bearing compression modulus to include the influence of the bulk modulus compressibility and the shape of the bearing cross section. The model includes the distributions of the compression modulus at the top and bottom boundaries expressed as Bessel functions.

The results of two types of severe loading tests of full-scale lead-rubber isolation bearings were used to show the validity of the refined model. The tests were a shear capacity limit-state test and a bi-directional, dynamic earthquake test. Negative incremental stiffness was observed in the hysteresis loops obtained from both tests, due to high axial load and large shear displacement. Simulation analyses were conducted for the tests. The influence of the $P-\Delta$ effect and compression modulus distribution on the bearing shear force-displacement hysteresis was examined. The best agreement between the experimental and analytical results was obtained when both the $P-\Delta$ effect and Bessel function compression modulus distribution were considered. The results comparisons indicate that the proposed model is useful for the prediction of the response of seismically-isolated structures under severe earthquake ground motions.

ACKNOWLEDGEMENT

The contribution of full-scale lead-rubber bearing test data by BC Hydro and Ausenco Sandwell is gratefully acknowledged. The simulation analyses were performed using a nonlinear structural analysis program, IDAC, developed by Shimizu Corporation, Japan. The research was partially supported by the Ministry of Education, Science, Sports and Culture, Grant-in-Aid for Scientific Research (B), 2011, 23360237. The authors would like to express their thanks to all of those who contributed to the research presented in this paper.

REFERENCES

- Kikuchi, M., Nakamura, T. and Aiken, I.D. (2010). Three-dimensional analysis for square seismic isolation bearings under large shear deformations and high axial loads. *Earthquake Engineering and Structural Dynamics*. **39**:1513-1531.
- Wada, A. and Hirose, K. (1989). Building frames subjected to 2D earthquake motion. *Structures Congress '89*. ASCE: 388-397.
- Kikuchi, M. and Aiken, I.D. (1997). An analytical hysteresis model for elastomeric seismic isolation bearings. *Earthquake Engineering and Structural Dynamics*. **26**:215-231.
- Kelly, J.M. (1997). *Earthquake-resistant Design with Rubber*. Springer: London, U.K.
- Sherstobitoff, J., Rezai, M., Aiken, I. and Yan, L. (2008). Seismic upgrade of an intake tower using underwater base isolation, preliminary design; Vancouver Island, Canada, *The 14th World Conference on Earthquake Engineering*: 05-06-0155.